Trends in Computational and Applied Mathematics, **27** (2026), e01852
Sociedade Brasileira de Matemática Aplicada e Computacional
Online version ISSN 2676-0029 www.scielo.br/tcam
ORIGINAL ARTICLE
doi: 10.5540/tcam.2026.027.e01852

Global instabilities of pyramidal trusses

W.T.M. SILVA[1], G.F. BARROZO[2] and A.A.A. PORTELA[3]

Received on February 10, 2025 / Accepted on February 13, 2026

ABSTRACT. This paper presents an exact analytical study of global instabilities in pyramidal trusses under large displacements. Using the stationarity of total potential energy and Green-Lagrange strain, nonlinear equilibrium equations are derived for a 3-bar isostatic truss. The tangent stiffness matrix yields 6 critical points: 2 limit points and 2 double bifurcation points. Multiple bifurcation is shown to occur universally for $\alpha > 45°$, independent of bar count $m \geq 3$ and alignment. Closed-form expressions for primary and secondary paths, validated via eigenvalue analysis, establish a generalized buckling threshold with direct implications for lightweight lattice design.

Keywords: multiple bifurcation, snap-through, pyramidal trusses.

1 INTRODUCTION

Pyramidal trusses, prized for their inherent geometric rigidity, high strength-to-weight ratio, and efficient load distribution, are becoming increasingly crucial across diverse engineering disciplines, including aerospace, mechanical engineering, energy absorption systems, and additive-manufactured metamaterials, [3].

Understanding the post-buckling behavior of structures is crucial for ensuring the safety and reliability of engineering designs. This paper presents a thorough exploration of the post-buckling behavior of pyramidal trusses, offering valuable insights into the stability of such structures under large displacements. The examination of static equilibrium analysis revealed the presence of multiple bifurcation phenomena, as evidenced by the identification of 6 critical points, 2 limit points, and 2 bifurcation points with a multiplicity of 2.

In structural analysis, bifurcation typically indicates a critical point where the structural behavior undergoes a qualitative change. The actual load-carrying capacity is often dictated by the characteristics of the bifurcation points within the ideal system. This is due to imperfections potentially

*Corresponding author: William Taylor Matias Silva – E-mail: taylor@unb.br
[1]Universidade de Brasília, Departamento de Engenharia Civil e Ambiental, Brasília, DF, Brazil – e-mail: taylor@unb.br https://orcid.org/0000-0002-8806-0440
[2]Universidade de Brasília, Departamento de Engenharia Civil e Ambiental, Brasília, DF, Brazil – e-mail: geovany.sh75@gmail.com https://orcid.org/0000-0003-1893-0735
[3]Universidade de Brasília, Departamento de Engenharia Civil e Ambiental, Brasília, DF, Brazil – e-mail: aportela@unb.br https://orcid.org/0000-0003-1342-1480

redirecting the solution path to a secondary route with significantly lower limit loads. Therefore, it is crucial to identify and scrutinize all secondary branches originating from a bifurcation point.

Early work on post-buckling analysis of critical points was presented by [12, 13], [8] and [7], where estimates on the number of branches from a critical point are given.

More recent work on post-buckling analysis of critical points was presented by [10], who introduced a method for analyzing and resolving symmetric bifurcations by formulating bifurcation equations through an asymptotic expansion approach. The derivation of these equations was carried out with a decomposition of spaces using the Lyapunov-Schmidt theory [6]. Other work on post-buckling analysis of critical points, relevant to this article, was presented by [5], who introduced an enhanced stiffness iteration method for the precise computation of bifurcation points with multiple zero eigenvalues.

While [10] and [5] developed numerical strategies for resolving symmetric and multiple bifurcations via asymptotic expansions and stiffness iteration, respectively, the present work derives *exact closed-form* equilibrium paths for the pyramidal truss. Unlike [9], who obtained analytical solutions under specific loading directions, we establish a *generalized buckling threshold* ($\alpha > 45°$) valid for arbitrary $m \geq 3$ and bar alignment, using symmetry and eigenvalue analysis of the tangent stiffness matrix.

The challenging problem of multiple bifurcation was presented by [14], who proposed a 4-degree-of-freedom benchmark model. The structure of multiple bifurcation points was studied by [1] in multi-folding microstructure models. A new method for finding multiple bifurcation points was presented by [11] using eigenvalue perturbation.

The stability of equilibrium configurations in pyramidal trusses was also investigated by [9], who analyzed elastic spatial trusses with regular pyramidal geometry. Exact closed-form solutions were derived for various loading conditions under linear elastic material behavior, small to moderate axial strains, and large nodal displacements. Despite their apparent geometric simplicity, these systems exhibit a rich variety of post-critical responses. The authors demonstrated that multiple bifurcation occurs exclusively under vertical loading, irrespective of the number of bars.

The organization of the paper is as follows. Section 2 describes the analytical formulation. Section 3 demonstrates that element misalignment does not alter multiple bifurcation. Section 4 shows that hyperstatic trusses exhibit the same behavior. Section 5 presents coalescence conditions. Section 6 describes primary and secondary paths. Section 7 presents conclusions.

2 ANALYTICAL FORMULATION

In order to analytically detect the critical points in the primary equilibrium path, this paper considers a pyramidal truss, as schematically represented in Figure 1. Pyramidal trusses represent the simplest generalization of the Mises truss to 3D space. Displacement boundary conditions, loading conditions as well as the geometrical properties of this pyramidal truss are also schematically represented in Figure 1. On the (x,y) plane draw a circle of radius R with

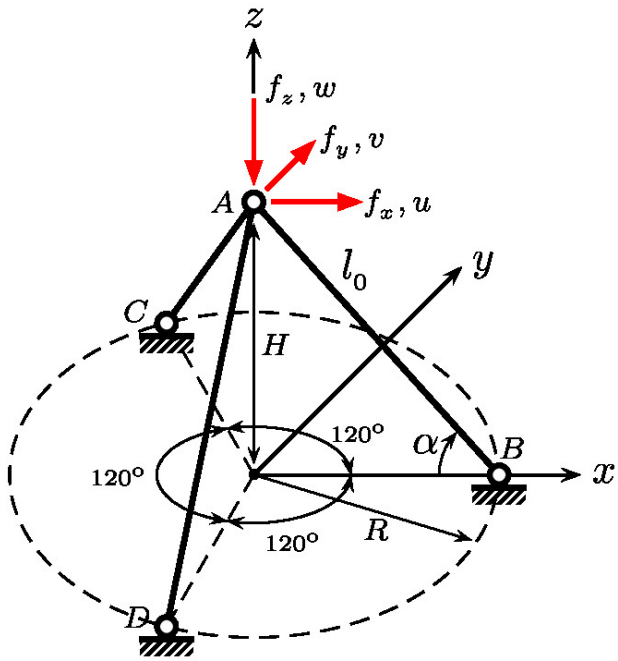

Figure 1: Isostatic pyramidal truss.

center at $x = y = 0$. Place $m \geq 3$ identical truss members going from the apex to the circle, spaced at equal circumferential angle $\phi = 2\pi/m$, and starting at the x axis. Figure 1 depicts the case $m = 3$, in which ϕ is 120^o. As outlined in [2, 4], an elastic linear constitutive model is employed to define the uniaxial stress-strain relationship, such that, $\sigma = E\varepsilon$, and the Green-Lagrange strain $\varepsilon = \frac{1}{2}(\frac{l^2}{l_0^2} - 1)$ is adopted as deformation measure. The axial rigidity of the each bar is EA_0. As represented in Figure 1, the initial length of each truss bar is given by $l_0 = \sqrt{R^2 + H^2}$, in which, $R = l_0 cos\alpha$ and $H = l_0 sin\alpha$. After the vertex displacement, given by (u, v, w), the current length of each bar will be given by $l_{AB} = \sqrt{(u-R)^2 + v^2 + (H-w)^2}$, $l_{AC} = \sqrt{(u + \frac{R}{2})^2 + (v - \frac{\sqrt{3}}{2}R)^2 + (H-w)^2}$ and $l_{AD} = \sqrt{(u + \frac{R}{2})^2 + (v + \frac{\sqrt{3}}{2}R)^2 + (H-w)^2}$, respectively. To make easier the algebraic development, the following non-dimensional parameters are adopted:

$$\mu_x = \frac{u}{l_0},\ \mu_y = \frac{v}{l_0},\ \mu_z = \frac{w}{l_0},\ \lambda_x = \frac{f_x}{EA_0},\ \lambda_y = \frac{f_y}{EA_0},\ \lambda_z = \frac{f_z}{EA_0} \tag{2.1}$$

Taking into account the definition of these parameters, as well as the definitions of l_0, l_{AB}, l_{AC} and l_{AD}, the Green-Lagrange strain of each bar element is given by

$$\begin{aligned}
\varepsilon_{AB} = \frac{l_{AB}^2 - l_0^2}{2l_0^2} &= \frac{(u-R)^2 + v^2 + (H-w)^2 - l_0^2}{2l_0^2} = \\
&= \tfrac{1}{2}\mu_x^2 + \tfrac{1}{2}\mu_y^2 + \tfrac{1}{2}\mu_z^2 - \mu_x cos\alpha - \mu_z sin\alpha \\
\varepsilon_{AC} = \frac{l_{AC}^2 - l_0^2}{2l_0^2} &= \frac{(u+\frac{R}{2})^2 + (v-\frac{\sqrt{3}}{2}R)^2 + (H-w)^2 - l_0^2}{2l_0^2} = \\
&= \tfrac{1}{2}\mu_x^2 + \tfrac{1}{2}\mu_y^2 + \tfrac{1}{2}\mu_z^2 + \tfrac{1}{2}\mu_x cos\alpha - \tfrac{\sqrt{3}}{2}\mu_y cos\alpha - \mu_z sin\alpha \\
\varepsilon_{AD} = \frac{l_{AD}^2 - l_0^2}{2l_0^2} &= \frac{(u+\frac{R}{2})^2 + (v+\frac{\sqrt{3}}{2}R)^2 + (H-w)^2 - l_0^2}{2l_0^2} = \\
&= \tfrac{1}{2}\mu_x^2 + \tfrac{1}{2}\mu_y^2 + \tfrac{1}{2}\mu_z^2 + \tfrac{1}{2}\mu_x cos\alpha + \tfrac{\sqrt{3}}{2}\mu_y cos\alpha - \mu_z sin\alpha
\end{aligned} \tag{2.2}$$

and, consequently, the total potential energy of the structural system is given by

$$\pi = EA_0 l_0 \left(\frac{1}{2}\varepsilon_{AB}^2 + \frac{1}{2}\varepsilon_{AC}^2 + \frac{1}{2}\varepsilon_{AD}^2 - \lambda_x\mu_x - \lambda_y\mu_y - \lambda_z\mu_z\right) \tag{2.3}$$

Since the structural system is considered only with 3 degrees of freedom, its equilibrium condition may be represented by a nonlinear system of 3 equations with 3 unknowns. The equation system can be found applying the principle of stationarity of the functional expressing the first variation of the total potential energy as $\delta\pi = \frac{\partial\pi}{\partial u_x}\delta u_x + \frac{\partial\pi}{\partial u_y}\delta u_y + \frac{\partial\pi}{\partial u_z}\delta u_z = 0$. Thus, taking into account the parameters defined in equation (2.1) and applying the condition of stationarity in the equation (2.3), the following system of equations is obtained:

$$\begin{aligned}
\mu_x(\varepsilon_{AB} + \varepsilon_{AC} + \varepsilon_{AD}) + cos\alpha\left(\tfrac{1}{2}(\varepsilon_{AC} + \varepsilon_{AD}) - \varepsilon_{AB}\right) - \lambda_x &= 0 \\
\mu_y(\varepsilon_{AB} + \varepsilon_{AC} + \varepsilon_{AD}) + \tfrac{\sqrt{3}}{2}cos\alpha(\varepsilon_{AD} - \varepsilon_{AC}) - \lambda_y &= 0 \\
(\mu_z - sin\alpha)(\varepsilon_{AB} + \varepsilon_{AC} + \varepsilon_{AD}) - \lambda_z &= 0
\end{aligned} \tag{2.4}$$

These equations represents the conditions of equilibrium, in the deformed configuration of the pyramidal truss, in the directions of the axes x, y and z, accordingly.

To obtain the tangent stiffness matrix, the load parameters are differentiated, relatively to the displacement parameters, in the equations of equilibrium, by considering that:

$$\begin{Bmatrix} d\lambda_x \\ d\lambda_y \\ d\lambda_z \end{Bmatrix} = \begin{bmatrix} \frac{\partial\lambda_x}{\partial\mu_x} & \frac{\partial\lambda_x}{\partial\mu_y} & \frac{\partial\lambda_x}{\partial\mu_z} \\ \frac{\partial\lambda_y}{\partial\mu_x} & \frac{\partial\lambda_y}{\partial\mu_y} & \frac{\partial\lambda_y}{\partial\mu_z} \\ \frac{\partial\lambda_z}{\partial\mu_x} & \frac{\partial\lambda_z}{\partial\mu_y} & \frac{\partial\lambda_z}{\partial\mu_z} \end{bmatrix} \begin{Bmatrix} d\mu_x \\ d\mu_y \\ d\mu_z \end{Bmatrix} \tag{2.5}$$

Hence, the coefficients of the tangent stiffness matrix are determined by differentiating the equations (2.2) and (2.4), in accordance to equation (2.5). After some basic algebraic developments, it follows that

$$\begin{Bmatrix} d\lambda_x \\ d\lambda_y \\ d\lambda_z \end{Bmatrix} = \begin{bmatrix} 3\mu_x^2 + \frac{3}{2}cos^2\alpha + \bar{\varepsilon} & 3\mu_x\mu_y & 3\mu_x(\mu_z - sin\alpha) \\ 3\mu_x\mu_y & 3\mu_y^2 + \frac{3}{2}cos^2\alpha + \bar{\varepsilon} & 3\mu_y(\mu_z - sin\alpha) \\ 3\mu_x(\mu_z - sin\alpha) & 3\mu_y(\mu_z - sin\alpha) & 3(\mu_z - sin\alpha)^2 + \bar{\varepsilon} \end{bmatrix} \begin{Bmatrix} d\mu_x \\ d\mu_y \\ d\mu_z \end{Bmatrix} \tag{2.6}$$

in which, $\bar{\varepsilon} = \varepsilon_{AB} + \varepsilon_{AC} + \varepsilon_{AD}$.

2.1 Tangent stiffness determinant and eigenvalues on primary path

Closed-form solutions can now be obtained for the determinant and eigenvalues of the tangent stiffness matrix. They will be used to detect and classify critical points on the primary equilibrium path. Critical points are characterized as limit points or bifurcation points. A limit point represents the loss of stiffness of the structural system when reaching the maximum load. After this critical point, the structural system becomes unstable and then, a dynamic jump occurs, in search of a stable equilibrium configuration. This phenomenon is known as *Snap-through*. The bifurcation point represents the buckling of the structural system, that is, a sudden change in the equilibrium path. To determine the critical points in the primary path, the following restrictions are imposed to the system: μ_x=μ_y=0 and λ_x=λ_y= 0, which leads to: ε_{AB}= ε_{AC}= ε_{AD}=$\varepsilon = \frac{1}{2}\mu_z^2 - \mu_z sin\alpha$, according to equations (2.2). When these restrictions are imposed in equation (2.6), the following expression of the tangent stiffness is obtained

$$\boldsymbol{K} = \begin{bmatrix} \frac{3}{2}cos^2\alpha + 3\varepsilon & 0 & 0 \\ 0 & \frac{3}{2}cos^2\alpha + 3\varepsilon & 0 \\ 0 & 0 & 3(\mu_z - sin\alpha)^2 + 3\varepsilon \end{bmatrix} \tag{2.7}$$

whose determinant is given by

$$det\ \boldsymbol{K} = (\tfrac{3}{2}\mu_z^2 - 3\mu_z sin\alpha + \tfrac{3}{2}cos^2\alpha)^2 (\tfrac{9}{2}\mu_z^2 - 9\mu_z sin\alpha + 3sin^2\alpha) = 0 \tag{2.8}$$

This is a polynomial of the 6th degree, with respect to μ_z, which can have 6 real roots. Note that two roots have multiplicity 2 because the coeficients k_{11} and k_{22} of the tangent matrix in (2.7) are equals, what imply in the multiple bifurcation. Since the tangent stiffness matrix, expressed in equation (2.7), is a diagonal, its pivots are therefore its eigenvalues, that are expressed as

$$\begin{aligned} \wp_1 = k_{11} &= \tfrac{3}{2}\mu_z^2 - 3\mu_z sin\alpha + \tfrac{3}{2}cos^2\alpha \\ \wp_2 = k_{22} &= \tfrac{3}{2}\mu_z^2 - 3\mu_z sin\alpha + \tfrac{3}{2}cos^2\alpha \\ \wp_3 = k_{33} &= \tfrac{9}{2}\mu_z^2 - 9\mu_z sin\alpha + 3sin^2\alpha \end{aligned} \tag{2.9}$$

These eigenvalues are polynomials of the 2nd degree, with respect to μ_z, whose roots are the critical points.

Table 1: Critical points.

critical point (1)	root 1 (2)	root 2 (3)	instability mode (4)
bifurcation point ($\wp_1$=0) $\alpha > 45^o$	$\mu_z^{bp_1} = sin\alpha - \sqrt{2sin\alpha^2 - 1}$	$\mu_z^{bp_2} = sin\alpha + \sqrt{2sin\alpha^2 - 1}$	spatial bifurcation buckling in the x-direction $\mu_x \neq 0$, $\mu_y = 0$ and $\mu_z \neq 0$
bifurcation point ($\wp_2$=0) $\alpha > 45^o$	$\mu_z^{bp_3} = sin\alpha - \sqrt{2sin\alpha^2 - 1}$	$\mu_z^{bp_4} = sin\alpha + \sqrt{2sin\alpha^2 - 1}$	spatial bifurcation buckling in the y-direction $\mu_x = 0$, $\mu_y \neq 0$ and $\mu_z \neq 0$
limit point ($\wp_3$=0)	$\mu_z^{lp_1} = (1 - \frac{\sqrt{3}}{3})sin\alpha$	$\mu_z^{lp_2} = (1 + \frac{\sqrt{3}}{3})sin\alpha$	Snap-through $\mu_x = 0$, $\mu_y = 0$ and $\mu_z \neq 0$

The roots of the polynomial in (2.9a), given by $\wp_1 = 0$, are relative to spatial buckling in the x direction, whereas the roots of the polynomial in (2.9b), given by $\wp_2 = 0$, are relative to spatial buckling in the y direction, and finally, the roots of the polynomial in (2.9c), given by $\wp_3 = 0$, are relative to the snap-through phenomenon. The values of these roots are presented in Table 1. Note that there are 6 critical points, which are 2 limit points and 2 bifurcation points of the multiplicity 2 that represent the multiple bifurcation.

For multiple bifurcation points to exist, the respective roots must be real. Therefore, for buckling in the x-direction or for buckling in the y-direction can take place when $\alpha > 45^o$ as shown in Table 1. It is observed that this condition is valid for any number of bars from $m \geq 3$, since the bars are spaced at equal circumferential angle $\phi = 2\pi/m$, as will be demonstrated in the next sections.

To study the behavior of the determinant and eigenvalues of the tangent stiffness matrix, along the primary equilibrium path, 3 models of the pyramidal truss will be analyzed. The radius of the circle will be the same for the 3 models, while the height will be different for each model. The definition of geometry and dimensionless parameters of each model are described in Table 2.

Table 2: Geometric parameters.

non-dimensional parameter (1)	model 1 $R = 3\,m, H = 2\,m$ (2)	model 2 $R = 3\,m, H = 4\,m$ (3)	model 3 $R = 3\,m, H = 6\,m$ (4)
α	33.69^o	53.13^o	63.43^o

Figures 2a, 2c and 2e show the graphs of the determinant, while Figures 2b, 2d and 2f show the graphs of the eigenvalues of the tangent stiffness for Models 1, 2 and 3 of the pyramidal truss, respectively. Regarding the graphs presented in these figures, it can be seen that:

- For Model 1, Figures 2a and 2b, there are only 2 real roots that represents the limit points lp_1 and lp_2. According the Figura 2b the multiple bifurcation not occur why $\wp_1$ and $\wp_2$ functions dont have real roots;
- For Model 2, Figures 2c and 2d, there are 6 real roots, 2 roots represent the limit points lp_1 and lp_2, and 2 roots of multiplicity 2 represent the bifurcation points bp_1, bp_2, bp_3 and bp_4, where $bp_1 = bp_3$ and $bp_2 = bp_4$. The multiple bifurcation occur before the limit point, $bp_1 = bp_3 < lp_1$. In the intervals $[bp_1 = bp_3, lp_1]$ and $[lp_2, bp_2 = bp_4]$ the determinant is positive but the equilibrium is unstable, since $\wp_1 < 0$ and $\wp_2 < 0$ in these intervals. When decreasing the value of the heigh H there is a tendency coalescence between $bp_1 = bp_3$ and lp_1, and $bp_2 = bp_4$ and lp_2, respectively;
- For Model 3, Figures 2e and 2f, there are 6 real roots, 2 roots represent the limit points lp_1 and lp_2, and 2 roots of multiplicity 2 represent the bifurcation points bp_1, bp_2, bp_3 and bp_4, where $bp_1 = bp_3$ and $bp_2 = bp_4$. The multiple bifurcation occur before the limit point, $bp_1 = bp_3 < lp_1$. In the intervals $[bp_1 = bp_3, lp_1]$ and $[lp_2, bp_2 = bp_4]$ the determinant is positive but the equilibrium is unstable, since $\wp_1 < 0$ and $\wp_2 < 0$ in these intervals. When increasing the value of the heigh H there is a tendency the increasing the gap between $bp_1 = bp_3$ and lp_1, and $bp_2 = bp_4$ and lp_2, respectively. The multiple bifurcation occurs long before the limit point.

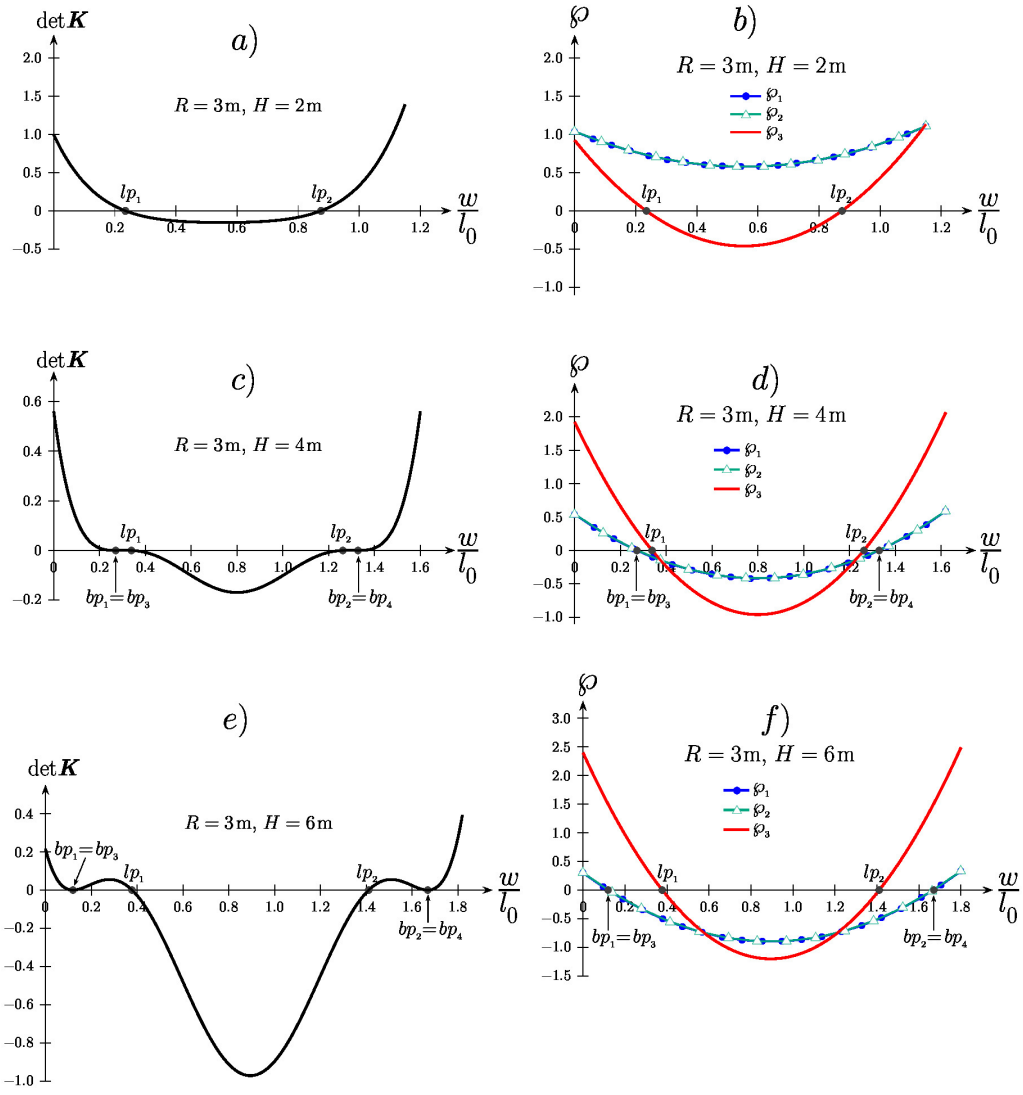

Figure 2: Determinant and eigenvalues of the tangent stiffness. a) and b) Model 1. c) and d) Model 2. e) and f) Model 3.

3 PYRAMIDAL TRUSS WITH THREE MEMBERS MISALIGNED WITH (X,Y) AXES

The objective in this section is to demonstrate that the misalignment of elements in the pyramidal truss concerning the x and y axes does not alter the value of the angle α at which multiple buckling occurs. This remains true as long as the angle ϕ between the projections of the elements in the (x,y) plane is consistent, specifically $\phi = 120^o$, as illustrated in Figure 3. In this scenario,

it is assumed that the projections of elements AB and AD are 15^o away from the x and y axes, respectively, while the projection of element AC is 45^o away from the y-axis.

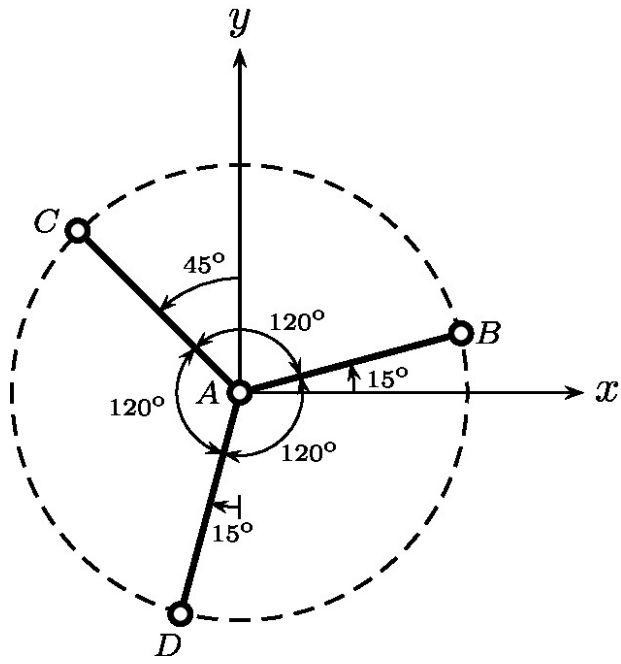

Figure 3: Members of the pyramidal truss projected on (x,y) plane.

Taking into account the coordinates of nodes A, B, C, and D in the undeformed configuration, as well as the displacements (u,v,w) of node A, in addition to the dimensionless parameters defined in Equation 2.1, the deformations of the elements are expressed as

$$\begin{aligned}
\varepsilon_{AB} = \frac{l_{AB}^2 - l_0^2}{2l_0^2} &= \frac{(u - R cos15^o)^2 + (v - R sin15^o)^2 + (H-w)^2 - l_0^2}{2l_0^2} = \\
&= \tfrac{1}{2}\mu_x^2 + \tfrac{1}{2}\mu_y^2 + \tfrac{1}{2}\mu_z^2 - \mu_x cos\alpha cos15^o - \mu_y cos\alpha sin15^o - \mu_z sin\alpha \\
\varepsilon_{AC} = \frac{l_{AC}^2 - l_0^2}{2l_0^2} &= \frac{(u + R sin45^o)^2 + (v - R cos45^o)^2 + (H-w)^2 - l_0^2}{2l_0^2} = \\
&= \tfrac{1}{2}\mu_x^2 + \tfrac{1}{2}\mu_y^2 + \tfrac{1}{2}\mu_z^2 + \mu_x cos\alpha sin45^o - \mu_y cos\alpha cos45^o - \mu_z sin\alpha \\
\varepsilon_{AD} = \frac{l_{AD}^2 - l_0^2}{2l_0^2} &= \frac{(u + R sin15^o)^2 + (v + R cos15^o)^2 + (H-w)^2 - l_0^2}{2l_0^2} = \\
&= \tfrac{1}{2}\mu_x^2 + \tfrac{1}{2}\mu_y^2 + \tfrac{1}{2}\mu_z^2 + \mu_x cos\alpha sin15^o + \mu_y cos\alpha cos15^o - \mu_z sin\alpha
\end{aligned} \tag{3.1}$$

Applying the principle of stationarity to the first-order variation of the total potential energy functional, defined in Equation 2.3, leads to the equilibrium equations expressed as

$$\begin{aligned}
\mu_x(\varepsilon_{AB}+\varepsilon_{AC}+\varepsilon_{AD})+cos\alpha(sin45^o\varepsilon_{AC}+sin15^o\varepsilon_{AD}-cos15^o\varepsilon_{AB})-\lambda_x&=0\\
\mu_y(\varepsilon_{AB}+\varepsilon_{AC}+\varepsilon_{AD})+cos\alpha(cos15^o\varepsilon_{AD}-sin15^o\varepsilon_{AB}-cos45^o\varepsilon_{AC})-\lambda_y&=0\\
(\mu_z-sin\alpha)(\varepsilon_{AB}+\varepsilon_{AC}+\varepsilon_{AD})-\lambda_z&=0
\end{aligned} \tag{3.2}$$

Applying the algebraic procedure defined in Equation 2.5 to the equilibrium equations described in Equation 3.2 leads to the same stiffness matrix given in Equation 2.6, noting that $(sin45^o+sin15^o-cos15^o)=0$ and $(cos15^o-sin15^o-cos45^o)=0$. Therefore, by imposing the constraints $\mu_x=\mu_y=0$ and $\lambda_x=\lambda_y=0$, the same stiffness matrix given in Equation 2.7 is obtained. Consequently, the same eigenvalues defined in Equation 2.9 can be obtained whose roots are presented in Table 1. Therefore, $\alpha>45^o$ represents the necessary condition for multiple buckling to occur.

4 PYRAMIDAL TRUSS WITH FOUR MEMBERS ($M=4$)

The objective of this section is to demonstrate that the number of elements $m>3$, comprising the pyramidal truss, does not alter the value of the angle α at which multiple buckling occurs. This remains true as long as the angle ϕ between the projections of the elements in the (x,y) plane be the same, as illustrated in Figure 4.

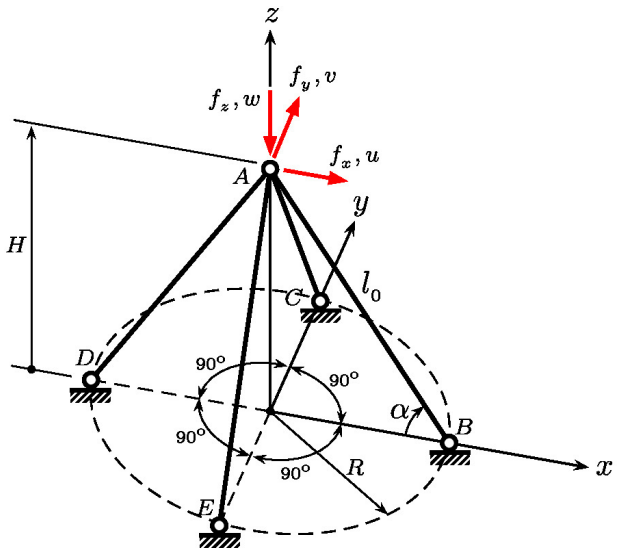

Figure 4: Pyramidal truss with four members.

For the sake of simplicity, consider the projections of the pyramidal truss elements in the (x,y) plane, composed of four elements aligned with the respective x and y axes, that is $\phi=90^o$,

as represented in Figure 4. Taking into account the coordinates of nodes A, B, C, D, and E in the undeformed configuration, as well as the displacements (u,v,w) at node A, along with the dimensionless parameters defined in Equation 2.1, the deformations of the elements are expressed as

$$\begin{aligned}
\varepsilon_{AB} = \frac{l_{AB}^2 - l_0^2}{2l_0^2} &= \frac{(u-R)^2+v^2+(H-w)^2-l_0^2}{2l_0^2} = \\
&= \tfrac{1}{2}\mu_x^2 + \tfrac{1}{2}\mu_y^2 + \tfrac{1}{2}\mu_z^2 - \mu_x cos\alpha - \mu_z sin\alpha \\
\varepsilon_{AC} = \frac{l_{AC}^2 - l_0^2}{2l_0^2} &= \frac{u^2+(v-R)^2+(H-w)^2-l_0^2}{2l_0^2} = \\
&= \tfrac{1}{2}\mu_x^2 + \tfrac{1}{2}\mu_y^2 + \tfrac{1}{2}\mu_z^2 - \mu_y cos\alpha - \mu_z sin\alpha \\
\varepsilon_{AD} = \frac{l_{AD}^2 - l_0^2}{2l_0^2} &= \frac{(u+R)^2+v^2+(H-w)^2-l_0^2}{2l_0^2} = \\
&= \tfrac{1}{2}\mu_x^2 + \tfrac{1}{2}\mu_y^2 + \tfrac{1}{2}\mu_z^2 + \mu_x cos\alpha - \mu_z sin\alpha \\
\varepsilon_{AE} = \frac{l_{AE}^2 - l_0^2}{2l_0^2} &= \frac{u^2+(v+R)^2+(H-w)^2-l_0^2}{2l_0^2} = \\
&= \tfrac{1}{2}\mu_x^2 + \tfrac{1}{2}\mu_y^2 + \tfrac{1}{2}\mu_z^2 + \mu_y cos\alpha - \mu_z sin\alpha
\end{aligned} \tag{4.1}$$

and, consequently, the total potential energy of the structural system is given by

$$\pi = EA_0 l_0 \left(\frac{1}{2}\varepsilon_{AB}^2 + \frac{1}{2}\varepsilon_{AC}^2 + \frac{1}{2}\varepsilon_{AD}^2 + \frac{1}{2}\varepsilon_{AE}^2 - \lambda_x\mu_x - \lambda_y\mu_y - \lambda_z\mu_z\right) \tag{4.2}$$

Taking into account the parameters defined in equation (2.1) and applying the condition of stationarity in the equation (4.2), the following system of equilibrium equations is obtained:

$$\begin{aligned}
\mu_x(\varepsilon_{AB}+\varepsilon_{AC}+\varepsilon_{AD}+\varepsilon_{AE}) + cos\alpha(\varepsilon_{AD}-\varepsilon_{AB}) - \lambda_x &= 0 \\
\mu_y(\varepsilon_{AB}+\varepsilon_{AC}+\varepsilon_{AD}+\varepsilon_{AE}) + cos\alpha(\varepsilon_{AE}-\varepsilon_{AC}) - \lambda_y &= 0 \\
(\mu_z - sin\alpha)(\varepsilon_{AB}+\varepsilon_{AC}+\varepsilon_{AD}+\varepsilon_{AE}) - \lambda_z &= 0
\end{aligned} \tag{4.3}$$

To obtain the tangent stiffness matrix, the load parameters are differentiated, relatively to the displacement parameters, in the equations of equilibrium, such that

$$\begin{Bmatrix} d\lambda_x \\ d\lambda_y \\ d\lambda_z \end{Bmatrix} = \begin{bmatrix} 4\mu_x^2 + 2cos^2\alpha + \bar{\varepsilon} & 4\mu_x\mu_y & 4\mu_x(\mu_z - sin\alpha) \\ 4\mu_x\mu_y & 4\mu_y^2 + 2cos^2\alpha + \bar{\varepsilon} & 4\mu_y(\mu_z - sin\alpha) \\ 4\mu_x(\mu_z - sin\alpha) & 4\mu_y(\mu_z - sin\alpha) & 4(\mu_z - sin\alpha)^2 + \bar{\varepsilon} \end{bmatrix} \begin{Bmatrix} d\mu_x \\ d\mu_y \\ d\mu_z \end{Bmatrix} \tag{4.4}$$

in which $\bar{\varepsilon} = \varepsilon_{AB} + \varepsilon_{AC} + \varepsilon_{AD} + \varepsilon_{AE}$. To determine the critical points in the primary path, the following restrictions are imposed to the system: μ_x=μ_y=0 and λ_x=λ_y= 0, which leads to: ε_{AB}= ε_{AC}= ε_{AD}= ε_{AE} = $\varepsilon = \frac{1}{2}\mu_z^2 - \mu_z sin\alpha$, according to equations (4.1). When these restrictions are imposed in equation (4.4), the following expression of the tangent stiffness is obtained

$$\boldsymbol{K} = \begin{bmatrix} 2cos^2\alpha + 4\varepsilon & 0 & 0 \\ 0 & 2cos^2\alpha + 4\varepsilon & 0 \\ 0 & 0 & 4(\mu_z - sin\alpha)^2 + 4\varepsilon \end{bmatrix} \tag{4.5}$$

whose eigenvalues are given by

$$\begin{aligned} \wp_1 = k_{11} &= 2\mu_z^2 - 4\mu_z sin\alpha + 2cos^2\alpha \\ \wp_2 = k_{22} &= 2\mu_z^2 - 4\mu_z sin\alpha + 2cos^2\alpha \\ \wp_3 = k_{33} &= 6\mu_z^2 - 12\mu_z sin\alpha + 4sin^2\alpha \end{aligned} \tag{4.6}$$

Note that $\wp_1 = \wp_2$, what imply in the multiple bifurcation. The roots of the polynomials in 4.6 represent the critical points in primary path. Therefore, $\wp_1 = \wp_2 = 0 \Rightarrow \mu_z^{bp_1} = \mu_z^{bp_3} = sin\alpha - \sqrt{2sin\alpha^2 - 1}$ and $\mu_z^{bp_2} = \mu_z^{bp_4} = sin\alpha + \sqrt{2sin\alpha^2 - 1}$. Note that these are the same values presented in Table 1. Therefore, for multiple buckling to occur, it is necessary that $2sin\alpha^2 - 1 > 0 \Longrightarrow \alpha > 45^o$, c.q.d., for $\forall\, m \geq 3$ and $\phi = 2\pi/m$.

5 COALESCENCE BETWEEN CRITICAL POINTS

The coalescence between critical points, given in Table 1, ocurr when $\mu_z^{bp_1} = \mu_z^{bp_3} = \mu_z^{lp_1}$ and $\mu_z^{bp_2} = \mu_z^{bp_4} = \mu_z^{lp_2}$, respectively, which implies in $sin\alpha = \sqrt{\frac{3}{5}}$, $\alpha = sin^{ß-1}(\sqrt{\frac{3}{5}}) = 50.77^o$ and $H = \sqrt{\frac{3}{2}}R$.

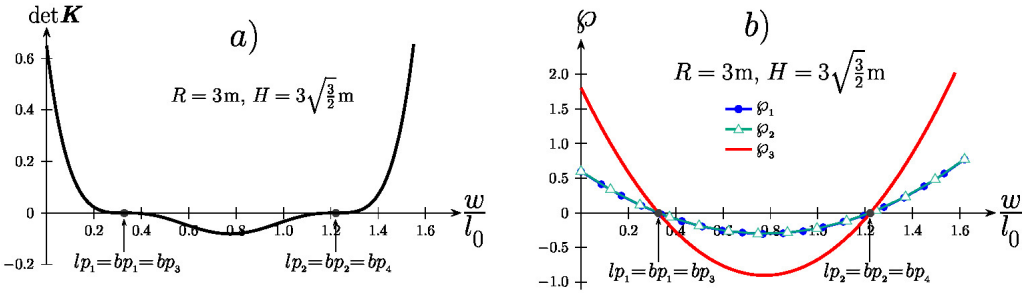

Figure 5: Determinant and eigenvalues of the tangent stiffness at critical points coalescence.

Figure 5a shows that the determinant has 2 real roots, of multiplicity 3, in which two of them represent limit points. There are 2 roots, that represent bifurcation points, of multiplicity 2 due to the coincidence of $bp_1 = pb_3$ and $bp_2 = pb_4$. Note that the curve of the determinant is tangent to the abscissa axis at the bifurcation points. Figure 5b shows the coincidence between the curves that represent the eigenvalues $\wp_1$ and $\wp_2$. Figure 5b shows the eigenvalues functions, where the coalescence between the critical points bp_1, bp_3 and lp_1, and between the points bp_2, bp_4 and lp_2 is evident.

The load factor at the bifurcations points, bp_1 or bp_3, is obtained by substituting the values the $\mu_z^{bp_1}$ or $\mu_z^{bp_3}$ given in Table 1 into equation 6.1 whose expression is $\lambda_z^{bp_{1,3}} = \frac{3}{2}(1 - sin^2\alpha)\sqrt{2sin^2\alpha - 1}$. Being that $sin\alpha = \frac{H}{\sqrt{H^2+R^2}}$, this equation can be rewritten as $\lambda_z^{bp_{1,3}} = \frac{3}{2}\frac{R^2\sqrt{H^2-R^2}}{(H^2+R^2)^{3/2}}$ depending on height and radius of the supports circle of the pyramidal truss. The Figure 6 shows the maximum load capacity at the bifurcation point for pyramidal trusses with

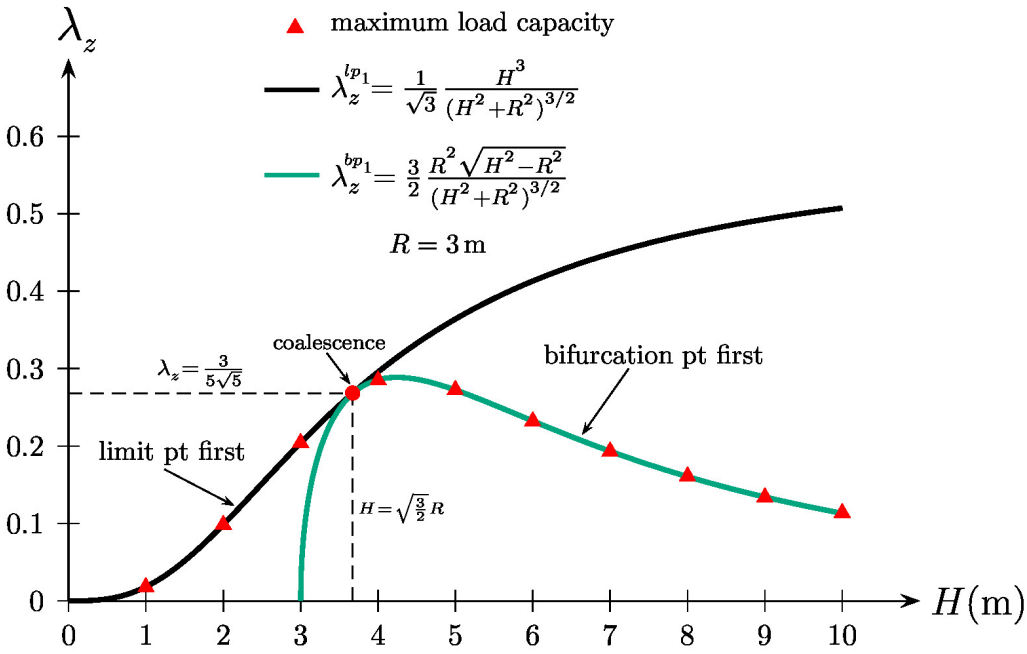

Figure 6: Maximum load capacity at the critical points for pyramidal trusses with different heights.

different heights adopting $R = 3\,m$. Note that the multiple bifurcation occur for $H > 3\,m$. For $H = 3.67\,m$ occur the coalescence between critical points. For $H > 3.67\,m$ the multiple bifurcation occur first. For $H < 3.67\,m$ the limit point occur first. The load factor at the limit point, lp_1, is obtained by substituting the value the $\mu_z^{lp_1}$ given in Table 1 into equation 6.1 whose expression is $\lambda_z^{lp_1} = \frac{1}{\sqrt{3}} sin^3\alpha$. This expression can be rewritten as a function of the height and of the radius as $\lambda_z^{lp_1} = \frac{1}{\sqrt{3}} \frac{H^3}{(H^2+R^2)^{3/2}}$. The Figure 6 shows the maximum load capacity at limit point for pyramidal trusses with different heights adopting $R = 3\,m$.

6 PRIMARY AND SECONDARY PATHS OF THE ISOSTATIC PYRAMIDAL TRUSS

By imposing the following conditions, μ_x=μ_y=0 and λ_x=λ_y=0, on equations 2.4, and according to equations 2.2, the primary equilibrium path is obtained as

$$\lambda_z = \frac{3}{2}\mu_z(\mu_z - sin\alpha)(\mu_z - 2sin\alpha) \tag{6.1}$$

This path is a polynomial of the 3rd degree, in terms of the parameter μ_z, whose graph is shown in Figure 7 for Model 2 of the isostatic pyramidal truss. As presented in Figure 7, the equilibrium path shows two extremes limit points, respectively lp_1 and lp_2. These points are determined with condition $d\lambda_z/d\mu_z = 0$, which leads to $\mu_z^{ßlp_1} = (1 - \frac{1}{\sqrt{3}})sin\alpha$ and $\mu_z^{ßlp_2} = (1 + \frac{1}{\sqrt{3}})sin\alpha$; substituting these values into equation (6.1), one obtains the values of these extremes which

are, respectively $\lambda_z^{lp_1} = \frac{1}{\sqrt{3}} sin^3\alpha$ and $\lambda_z^{lp_2} = -\frac{1}{\sqrt{3}} sin^3\alpha$. Table 3 shows the values of these limit points for Model 2 of the pyramidal truss.

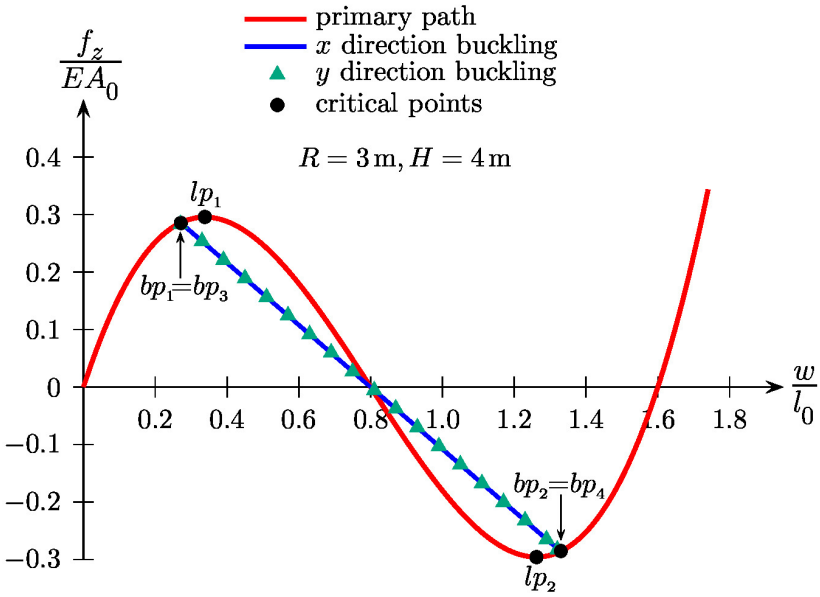

Figure 7: Snap-through and secondary paths.

Table 3: Limit points. Model 2.

root 1	load factor	root 2	load factor
$\mu_z^{\beta lp_1}$	$\lambda_z^{lp_1}$	$\mu_z^{\beta lp_2}$	$\lambda_z^{lp_2}$
(1)	(2)	(3)	(4)
0.3381	0.2956	1.2619	-0.2956

6.1 Multiple bifurcation

This section describes the phenomenon of multiple bifurcation of the pyramidal trusss. Buckling can occur in the x-axis direction as well as in the y-axis direction. It is important to highlight that the buckling occurs symmetrically in the x and y-directions due to rotational symmetry of the pyramidal truss.

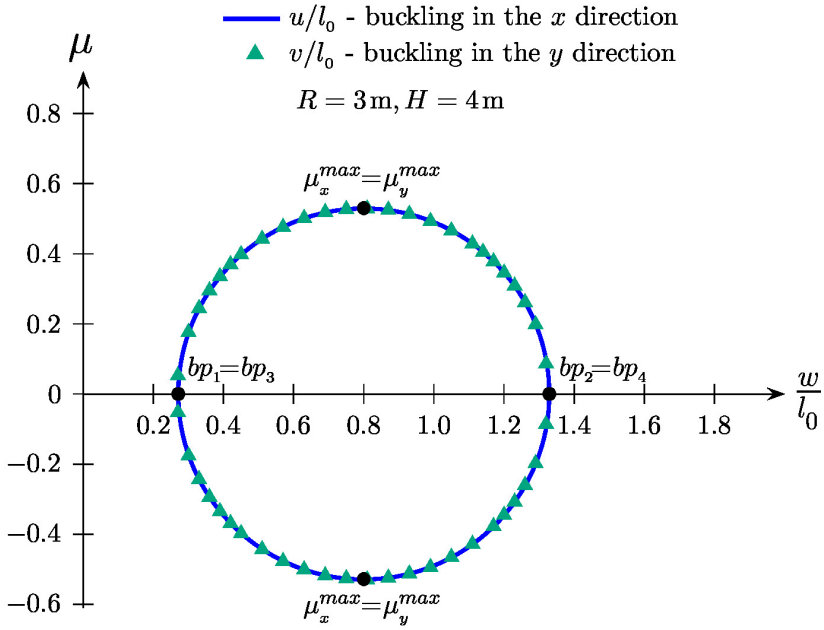

Figure 8: Secondary paths: μ_xß×μ_z and μ_yß×μ_z.

6.1.1 Buckling in the x direction

The buckling in the x direction is simulated imposing the conditions: $\mu_x \neq 0$, $\mu_y = 0$, $\mu_z \neq 0$, $\lambda_x = 0$ and $\lambda_y = 0$. When these restrictions are introduced in equations (2.4), the system of equations

$$\begin{aligned} \mu_x(\varepsilon_{AB}+\varepsilon_{AC}+\varepsilon_{AD}) + cos\alpha(\tfrac{1}{2}(\varepsilon_{AC}+\varepsilon_{AD}) - \varepsilon_{AB}) &= 0 \\ (\mu_z - sin\alpha)(\varepsilon_{AB}+\varepsilon_{AC}+\varepsilon_{AD}) - \lambda_z &= 0 \end{aligned} \tag{6.2}$$

can be obtained. In addition, taking into account equations (2.2), those restrictions lead to, respectively $\varepsilon_{AB}+\varepsilon_{AC}+\varepsilon_{AD} = \frac{3}{2}\mu_x^2 + \frac{3}{2}\mu_z^2 - 3\mu_z sin\alpha$ and $\frac{1}{2}(\varepsilon_{AC}+\varepsilon_{AD}) - \varepsilon_{AB} = \frac{3}{2}\mu_x cos\alpha$. When these expressions are introduced in equation (6.2a), the constraint $\mu_x(\frac{3}{2}\mu_x^2 + \frac{3}{2}\mu_z^2 - 3\mu_z sin\alpha + \frac{3}{2}cos^2\alpha) = 0$ is obtained. This constraint can be satisfied through 2 conditions, which are either $\mu_x = 0$ or $\mu_x^2 + \mu_z^2 - 2\mu_z sin\alpha + cos^2\alpha = 0$. For the first condition, the primary equilibrium path takes place, while for the second condition, the buckling in the x direction takes place, provided that restrictions given in equations (6.3b) and (6.3c) are satisfied.

$$\begin{aligned} \mu_x = &\quad \pm\sqrt{-\mu_z^2 + 2\mu_z sin\alpha - cos^2\alpha} \\ sin\alpha - \sqrt{2sin^2\alpha - 1} < \mu_z < &\quad sin\alpha + \sqrt{2sin^2\alpha - 1} \\ sin\alpha > &\quad \tfrac{1}{\sqrt{2}} = 45^o \end{aligned} \tag{6.3}$$

Note that the extreme values of μ_z, in equation (6.3b), are the roots of the eigenvalue function $\wp_1$, presented in Table 1; for these roots to be real, the condition given in (6.3c) must be satisfied. To

Table 4: Bifurcation points. Model 2.

root 1	load factor	root 2	load factor	root 3	load factor	root 4	load factor
$\mu_z^{ßbp_1}$	$\lambda_z^{bp_1}$	$\mu_z^{ßbp_2}$	$\lambda_z^{bp_2}$	$\mu_z^{ßbp_3}$	$\lambda_z^{bp_3}$	$\mu_z^{ßbp_4}$	$\lambda_z^{bp_4}$
(1)	(2)	(3)	(4)	(5)	(6)	(7)	(8)
0.2709	0.2857	1.3292	-0.2857	0.2709	0.2857	1.3292	-0.2857

obtain the secondary path, the constraints in (6.3a) and $\varepsilon_{AB}+\varepsilon_{AC}+\varepsilon_{AD}=\frac{3}{2}\mu_x^2+\frac{3}{2}\mu_z^2-3\mu_z sin\alpha$ are replaced in equation (6.2b), which leads to

$$\lambda_z=\frac{3}{2}cos^2\alpha(sin\alpha-\mu_z) \tag{6.4}$$

This is the equation of the line, function of the parameter μ_z, whose graph is shown in Figure 7.

When the extreme values of μ_z, given by the equation (6.3b), are replaced in equation (6.4), one get the load factors $\lambda_z^{bp_1}=\frac{3}{2}cos^2\alpha\sqrt{2sin^2\alpha-1}$ and $\lambda_z^{bp_2}=-\frac{3}{2}cos^2\alpha\sqrt{2sin^2\alpha-1}$, respectively. Table 4 shows the values of these bifurcation points for the pyramidal truss, Model 2.

The maximum displacement in (6.3a) is given by $\frac{d\mu_x}{d\mu_z}=0\Rightarrow\mu_x^{max}=\pm\sqrt{2sin^2\alpha-1}$. Figure 8 shows after the bifurcation, represented by point bp_1, the displacement μ_x of the vertex of the pyramidal truss increases until a maximum of $\pm\frac{\sqrt{7}}{5}$. After reaching this maximum, the displacement decreases until it cancels out at point bp_2. This point indicates that the pyramidal truss returns to the primary path, as can also be seen in the Figure 7.

6.1.2 Buckling in the *y* direction

The buckling in the *y* direction is simulated imposing the conditions: $\mu_x=0$, $\mu_y\neq 0$, $\mu_z\neq 0$, $\lambda_x=0$ and $\lambda_y=0$. When these restrictions are introduced in equations (2.4), the system of equations

$$\begin{aligned} 3\mu_y\varepsilon_{AB}+\tfrac{\sqrt{3}}{2}cos\alpha(\varepsilon_{AD}-\varepsilon_{AC})&=0\\ 3(\mu_z-sin\alpha)\varepsilon_{AB}-\lambda_z&=0\end{aligned} \tag{6.5}$$

can be obtained. In addition, taking into account equations (2.2), the following relations are obtained $\varepsilon_{AD}-\varepsilon_{AC}=\sqrt{3}\mu_y cos\alpha$ and $\varepsilon_{AB}=\frac{1}{2}\mu_y^2+\frac{1}{2}\mu_z^2-\mu_z sin\alpha$, respectively. When these expressions are introduced in equation (6.5a), the constraint $3\mu_y(\frac{1}{2}\mu_y^2+\frac{1}{2}\mu_z^2-\mu_z sin\alpha+\frac{1}{2}cos^2\alpha)=0$ is obtained. This constraint can be satisfied through 2 conditions, which are either $\mu_y=0$ or $\mu_y^2+\mu_z^2-2\mu_z sin\alpha+cos^2\alpha=0$. For the first condition, the primary equilibrium path takes place, while for the second condition, the buckling in the *y* direction takes place, provided that restrictions given in equations (6.6b) and (6.6c) are satisfied.

$$\begin{aligned} \mu_y = &\quad \pm\sqrt{-\mu_z^2 + 2\mu_z sin\alpha - cos^2\alpha} \\ sin\alpha - \sqrt{2sin^2\alpha - 1} < \mu_z < &\quad sin\alpha + \sqrt{2sin^2\alpha - 1} \\ sin\alpha > &\quad \tfrac{1}{\sqrt{2}} = 45^o \end{aligned} \tag{6.6}$$

Note that the extreme values of μ_z, in equation (6.6b), are the roots of the eigenvalue function $\wp_2$, presented in Table 1; for these roots to be real, the condition given in (6.6c) must be satisfied. To obtain the secondary path, the constraints in (6.6a) and $\varepsilon_{AB} = \frac{1}{2}\mu_y^2 + \frac{1}{2}\mu_z^2 - \mu_z sin\alpha$ are replaced in equation (6.5b), which leads to

$$\lambda_z = \frac{3}{2} cos^2\alpha (sin\alpha - \mu_z) \tag{6.7}$$

This is the equation of the line, function of the parameter μ_z, whose graph is shown in Figure 8. Note that equations (6.6) and (6.7) are equal to equations (6.3) and (6.4), respectively. When the extreme values of μ_z, given by the equation (6.6b), are replaced in equation (6.7), one get the load factors $\lambda_z^{bp_3} = \frac{3}{2} cos^2\alpha\sqrt{2sin^2\alpha - 1}$ and $\lambda_z^{bp_4} = -\frac{3}{2} cos^2\alpha\sqrt{2sin^2\alpha - 1}$, respectively. Table 4 shows the values of these bifurcation points for the pyramidal truss, Model 2.

The maximum displacement in (6.6a) is given by $\frac{d\mu_y}{d\mu_z} = 0 \Rightarrow \mu_y^{max} = \pm\sqrt{2sin^2\alpha - 1}$. Figure 8 shows after the bifurcation, represented by point bp_3, the displacement μ_y of the vertex of the pyramidal truss increases until a maximum of $\pm\frac{\sqrt{7}}{5}$. After reaching this maximum, the displacement decreases until it cancels out at point bp_4. This point indicates that the pyramidal truss returns to the primary path, as can also be seen in the Figure 7.

7 CONCLUSIONS

The findings of this research significantly advance the understanding of post-buckling behavior in pyramidal trusses, a class of lightweight spatial structures increasingly employed in aerospace, civil, and mechanical engineering applications. Through rigorous static equilibrium analysis, we have identified six critical points on the primary equilibrium path—comprising two limit points and two double bifurcation points—revealing a rich landscape of global instability phenomena under large displacements. A key contribution is the establishment of a generalized buckling criterion: multiple bifurcation occurs universally for $\alpha > 45°$, independent of the number of bars $m \geq 3$ and their planar alignment, provided the angular spacing remains $2\pi/m$. This threshold represents a fundamental geometric condition governing the onset of complex post-critical responses, extending beyond the specific loading scenarios previously analyzed in the literature.

The analytical framework, rooted in the stationarity of total potential energy, Green-Lagrange strain kinematics, and exact derivation of the tangent stiffness matrix, provides closed-form expressions for both primary and secondary equilibrium paths. These solutions, validated through eigenvalue analysis and numerical path-following, offer precise predictions of snap-through and transverse buckling modes. The symmetry-based reduction of the bifurcation problem, exploit-

ing rotational invariance in the x- and y-directions, further enhances computational efficiency and physical insight.

While the present study focuses on the isostatic configuration with three bars, the modular nature of the formulation lays a robust foundation for extension to hyperstatic pyramidal lattices. Future developments will involve systematic assembly of element stiffness matrices, incorporation of higher-order symmetry groups, and exploration of dynamic snap-through, imperfection sensitivity, and topology optimization for enhanced energy absorption in metamaterials and deployable structures.

In conclusion, this work not only deepens the theoretical understanding of multiple bifurcation and global instability in three-dimensional truss systems but also delivers practical, analytically tractable tools for engineers. The derived instability maps, critical load formulas, and geometric thresholds enable proactive design against undesirable post-buckling modes, thereby contributing to safer, more reliable, and efficient structural systems in advanced engineering applications.

Data availability

All data generated or analysed during this study are included in this published article.

Associate editor: Antônio José Silva Neto

REFERENCES

[1] I. Ario & M. Nakazawa. Analysis of multiple bifurcation behavior for periodic structures. *Archives of Mechanics*, **72**(4) (2020), 283–306. doi:10.24423/aom.3433.

[2] J. Bonet, A.J. Gil & R.D. Wood. "Nonlinear solid mechanics for finite element analysis: Statics". Cambridge University Press (2016).

[3] J. Bühring, M. Nuño & K.U. Schröder. Additive-manufactured sandwich structures: Mechanical characterization and usage potential in small aircraft. *Aerospace Science and Technology*, **111** (2021), 106548. doi:10.1016/j.ast.2021.106548.

[4] M.A. Crisfield. "Non-linear finite element analysis of solids and structures, Volume 1: Essentials". John Wiley & Sons (1991).

[5] F. Fujii, K. Ikeda, H. Noguchi & S. Okazawa. Modified stiffness iteration to pinpoint multiple bifurcation points. *Computer Methods in Applied Mechanics and Engineering*, **190**(18-19) (2001), 2499–2522. doi:10.1016/S0045-7825(00)00249-8.

[6] M. Golubitsky & D.G. Schaeffer. "Singularities and Groups in Bifurcation Theory. Volume I". Springer-Verlag (1985).

[7] K.C. Johns. Simultaneous buckling in symmetric structural systems. *Journal of the Engineering Mechanics Division*, **98**(4) (1972), 835–848. doi:10.1061/JMCEA3.0001641.

[8] K.C. Johns & A.H. Chilver. Multiple path generation at coincident branching points. *International Journal of Mechanical Sciences*, **13**(11) (1971), 899–910. doi:10.1016/0020-7403(71)90076-2.

[9] S.S. Ligarò & P.S. Valvo. Large displacement analysis of elastic pyramidal trusses. *International Journal of Solids and Structures*, **43** (2006), 4867–4887. doi:10.1016/j.ijsolstr.2005.06.100.

[10] A. Magnusson. Analysis of post-buckling branches at multiple symmetric bifurcations. *International Journal for Numerical Methods in Engineering*, **51**(4) (2001), 413–428. doi:10.1002/nme.157.

[11] M. Rezaiee-Pajand & H.R. Vejdani-Noghreiyan. Computation of multiple bifurcation point. *Engineering Computations. International journal for computer-aided engineering and software*, **23**(5) (2006), 552–565. doi:10.1108/02644400610671135.

[12] M.J. Sewell. A general theory of equilibrium paths through critical points. *Proceedings of the Royal Society A*, **306**(1485) (1968), 201–238. doi:10.1098/rspa.1968.0146.

[13] M.J. Sewell. On the branching of equilibrium paths. *Proceedings of the Royal Society A*, **315**(1523) (1970), 499–518. doi:10.1098/rspa.1970.0058.

[14] M. Tanaka, K. Ikeda, K.M. Hsiao & F. Fujii. Mathematical design and graphical solution of the multiple bifurcation equations of a 4-DoF benchmark model. *Thin-Walled Structures*, **166** (2021), 108010. doi:10.1016/j.tws.2021.108010.

How to cite

W.T.M. Silva, G.F. Barrozo & A.A.A. Portela. Global instabilities of pyramidal trusses. *Trends in Computational and Applied Mathematics*, **27**(2026), e01852. doi: 10.5540/tcam.2026.027.e01852.